Food Chemistry 173 (2015) 725–732

Contents lists available at ScienceDirect

Food Chemistry

journal homepage: www.elsevier.com/locate/foodchem

Photoproducts of carminic acid formed by a composite from *Manihot dulcis* waste

Cynthia M. Antonio-Cisneros [a,b], Martín M. Dávila-Jiménez [c], María P. Elizalde-González [a,*], Esmeralda García-Díaz [a]

[a] Centro de Química, Instituto de Ciencias, Universidad Autónoma de Puebla, Ciudad Universitaria, Edif. 103H, Puebla, Pue. 72570, Mexico
[b] Instituto de Agroingeniería, Universidad del Papaloapan, Campus Loma Bonita, Oaxaca, Mexico
[c] Facultad de Ciencias Químicas, Universidad Autónoma de Puebla, Ciudad Universitaria, Edif. 105, Puebla, Pue. 72570, Mexico

ARTICLE INFO

Article history:
Received 29 July 2014
Received in revised form 6 October 2014
Accepted 16 October 2014
Available online 22 October 2014

Keywords:
Natural red 4
Carminic acid
Photolysis
Photocatalysis
Product identification
Manihot waste
TiO_2/carbon composite

ABSTRACT

Carbon–TiO_2 composites were obtained from carbonised *Manihot dulcis* waste and TiO_2 using glycerol as an additive and thermally treating the composites at 800 °C. Furthermore, carbon was obtained from *manihot* to study the adsorption, desorption and photocatalysis of carminic acid on these materials. Carminic acid, a natural dye extracted from cochineal insects, is a pollutant produced by the food industry and handicrafts. Its photocatalysis was observed under different atmospheres, and kinetic curves were measured by both UV–Vis and HPLC for comparison, yielding interesting differences. The composite was capable of decomposing approximately 50% of the carminic acid under various conditions. The reaction was monitored by UV–Vis spectroscopy and LC-ESI-(Qq)-TOF-MS-DAD, enabling the identification of some intermediate species. The deleterious compound anthracene-9,10-dione was detected both in N_2 and air atmospheres.

© 2014 Elsevier Ltd. All rights reserved.

1. Introduction

Carminic acid (CA) is a natural dye extracted from cochineal insects that can yield shades of red. The Food Standards Agency in Europe and the United States Food and Drug Administration (FDA) have not banned its use in food. CA is also used in histology, as well as the coloring of pharmaceuticals, cosmetics, plastics and fabrics. Particularly in Oaxaca (Mexico), CA is also the most important insect-derived dye used in the production of rugs and handicrafts. During the fabrication of both food and hand-woven carpets, significant amounts of CA are released in the food industry and artisanal carpeting effluents. Fortunately, CA showed negative genotoxicity in a somatic mutation and recombination test of *Drosophila melanogaster* (Sarikaya, Selvi, & Erkoç, 2012).

If we consider the problem of removing CA by the most common technique used for dyes, adsorption (Rangabhashiyam, Anu, & Selvaraju, 2013), the only reports of such removal are early ones using activated carbon. In recent years, the application of adsorbents in this respect have focused on the recovery and purification of CA (Bibi, Galvis, Grasselli, & Fernández-Lahore, 2012; Cabrera & Fernandez-Lahore, 2007). In contrast to adsorption, heterogeneous photocatalysis can be regarded as a water purification process that can achieve mineralisation by producing, at times, toxic intermediates during degradation. Incidentally, authors reported observing a higher toxicity after the biodegradation of CA than before the microbiological treatment of effluent (Arroyo-Figueroa et al., 2011). The fact that hydroxylated anthraquinones have presented significant toxicity is important because these compounds can be photoproducts of CA (Brack et al., 2003). This fact makes the identification of the compounds produced during the degradation of CA necessary.

In the food industry, CA is considered not only a colorant that resists degradation over time but also one of the most light-stable, heat-stable and oxidation-resistant dyes among all natural dyestuffs. However, Jørgensen and Skibsted (1991) found that the photolability of CA increased with deprotonation and was enhanced with irradiation at 254 nm. Recently, Gosetti, Chiuminatto, Mazzucco, Mastroianni, and Marego (2015) studied the effect of sun irradiation on CA in aqueous solution and in sixteen different beverages to mimic the action of sunlight during transport. In the presence of TiO_2, authors degraded CA using UVA (366 nm) irradiation and demonstrated the adsorption of the dye onto the photocatalyst (Baran, Makowski, & Wardas, 2008). Furthermore, with the addition of H_2O_2, UV irradiation

* Corresponding author.
E-mail address: maria.elizalde.uap.mx@gmail.com (M.P. Elizalde-González).

http://dx.doi.org/10.1016/j.foodchem.2014.10.085
0308-8146/© 2014 Elsevier Ltd. All rights reserved.

caused a 60% decoloration of CA under optimised conditions (Körbahti & Rauf, 2009). In spectroscopic studies, CA also underwent degradation in its solid state by exposure to visible light under anoxic conditions (Koperska, Łojewski, & Łojewska, 2011). To date, the advancements in photocatalysis for the degradation of target substances are undeniable, due to the development of semiconductor materials. The photocatalytic removal of dyestuffs from water has been reviewed (Ahmed, Rasul, Martens, Brown, & Hashib, 2011; Akpan & Hameed, 2009), but the photocatalytic degradation of CA on TiO_2/carbon materials has not yet been addressed.

Combinations of TiO_2 and carbon are common composites in the field of photocatalysis (Leary & Westwood, 2011). In recent years, the application of these carbon–TiO_2 materials in photocatalysis has gained widespread attention because (i) the solids are easily recovered after use in a wide range of applications (Foo & Hameed, 2010) and (ii) synergistic effects occur between TiO_2 and carbon (Matos, Chovelon, Cordero, & Ferronato, 2009).

Only a few studies have been devoted to the preparation of TiO_2/carbon materials using lignocellulosic residues, such as bamboo leaves (Huang et al., 2011), pine sawdust (Asiltürk & Şener, 2012), maize corncob (Sabinas-Hernández, 2011), canola hull (Mahmoodi, Arami, & Zhang, 2011), corn straw powder (Chen et al., 2012), and *manihot* residues (Antonio Cisneros, 2010) as carbon precursors.

Our goal was to measure the sensitivity of aqueous solutions of CA to UV light under various conditions as well as the photolability of CA on TiO_2 immobilised on carbon obtained from dried stem residues *of Manihot dulcis* (sweet cassava). The present study focused on the LC–MS identification of intermediates produced by the irradiation of CA in the presence of a TiO_2/C800 composite rather than on the assessment of the mineralisation of CA.

2. Experimental

2.1. Chemicals

Carminic acid (C.I. 75470), also called crimson lake, cochineal, natural red 4, or E120, was purchased from Sigma Aldrich (St. Louis, MO; CAS 1260-17-9). The purity of CA, determined by HPLC was 94%. Glycerol (87% GR) was purchased from Merck (Darmstadt, Germany). Titanium oxide aeroxide P25, batch number 1036070711 (Degussa, Parsippany, NJ) was used for immobilisation on *manihot* carbon and was also used for comparative purposes. The natural pH value of the CA solutions was 5.7.

2.2. Immobilization of TiO_2 on carbon

Raw residues of *M. dulcis* stems without the rind or pith (0.45 mm sieved particles) dried at 70 °C for 24 h were used as the carbon precursor (Antonio Cisneros & Elizalde-González, 2010). The TiO_2/carbon composite was fabricated as follows. A glycerol suspension (10 mL) of *manihot* particles (10 g) was prepared by mixing with a TiO_2 aqueous slurry (10 mL). The resultant homogeneous suspension was maintained in a combustion boat at room temperature for 24 h. The temperature regime of the carbonisation consisted of two heating ramps, *viz.* from room temperature to 50 °C at 4 °C min^{-1}, then 1 h at 50 °C and from 50 °C to 800 °C at 4 °C min^{-1}. Then, the residues were maintained at the maximum temperature for 4 h. The oven was then allowed to cool to room temperature. A horizontal tubular furnace (Carbolite Furnaces Ltd, Hope Valley, UK) with a quartz reactor was used. A carbon sample not containing TiO_2, denoted C800, was used for comparison and was obtained by carbonising raw *manihot* particles. The same horizontal tubular furnace and heating program were used for the C800 sample as for the composite preparation.

2.3. Characterisation of the composite

The morphology and surface composition of the composite were determined using an Oxford Instruments INCAX-act Energy 350 EDS spectrometer coupled to a JEOL JSM 6610 LV scanning electron microscope (SEM). The BET surface area was measured by nitrogen adsorption at 77 K using an Autosorb-1 from Quantachrome Instruments (Boynton Beach, FL) after out-gassing at 573 K for 12 h. The specific surface area was calculated using the Brunauer–Emmett–Teller (BET) method, and the pore size distribution was estimated by the Barrett–Joyner–Halenda method (BJH). The extent of micro- and mesoporosity was calculated using the t-method. The specific surface area of the raw residues was determined by the adsorption of methylene blue using a molecular area of 1.35 nm^2 in the vertical orientation (Antonio-Cisneros, 2010). The density of the dry materials was determined in triplicate using tarred vessels. The point of zero charge (pH_{pzc}) was measured by methodology reported elsewhere (Bourikas, Vakros, Kordulis, & Lycourghiotis, 2003).

2.4. Adsorption and desorption experiments

Adsorption tests were performed at 25 °C in thermostatted batch experiments. The solid materials, raw *manihot* residues, carbon, and TiO_2/carbon composite with a particle size of 0.25 mm were dried for 24 h at 75 °C. Then, 100 mg of each material were weighed into polycarbonate cylindrical cells with lids and contacted at 25 °C with 3 mL of CA solutions with concentrations in the range of 100–3000 mg L^{-1}. The pH was not adjusted and was measured to be 5.7 in deionised water. The solution obtained after 24 h, resulting from adsorption equilibrium, was separated from the exhausted adsorbent, centrifuged (12,000 rpm) and then analysed with a Hach spectrophotometer at 495 nm (Hach Company, Loveland, CO). The adsorbed amount a was determined by measuring the final concentration C_f of CA in the solution and applying the formula $a = (C_0 - C_f)V/m$, where C_0 is the initial concentration of CA, V is the volume added (in litres), and m is the weighed mass (in grams).

Desorption measurements were carried out as follows. A saturated sample was separated from the solution by filtration. Then, it was dried at 90 °C for 12 h. Afterwards, the dried sample was weighed and placed in contact with 3 mL of deionized water in polycarbonate cylindrical cells at 25 °C for 24 h. The desorbed amount a_{des} was determined by measuring the concentration of CA in the solution produced by desorption C_{des} and applying the formula $a_{des} = (C_{des} \cdot V)/m$, where V is the volume added (in L) and m is the weighed mass (in grams). To determine the equilibrium concentrations, calibration curves with $r^2 = 0.999$ were obtained for both the adsorption and desorption experiments.

2.5. Photolysis and photocatalytic experiments

For the irradiation experiments performed on the composite and TiO_2 (Degussa P25), a 15-mL temperature-controlled quartz reactor from Ace Glass Inc. (Vineland, NJ) was used for the experiments involving irradiation at 254 nm. A $2\frac{1}{8}$-inch Pen-Ray light source (5.5 W) from Ultra-Violet Products (Upland, CA) was immersed into the reactor in a quartz jacket. The reactor was equipped with a water jacket to filter out the IR irradiation of the lamp and to control the temperature of the solution. A flow of chromatographic-grade dry air or nitrogen was allowed to bubble into the bulk solution. The entire assembly was enclosed in a dark chamber, and the lamp was switched on after 30 min to establish adsorption equilibrium. In each experiment, 10 mg of the composite were added to 10 mL of a solution containing 300 mg L^{-1} of CA. Aliquots were collected at regular time intervals during irradiation

and were centrifuged for 45 min before analysis. Samples of all of the CA solutions subjected to photocatalytic testing with the composite and TiO_2 were analysed using a Hach DR 5000 UV–Vis spectrophotometer over the wavelength range of 200–800 nm.

2.6. Analysis of the photocatalysis products

The collected aliquots were analyzed by liquid chromatography using an LC–MS instrument (Series 1260 chromatograph coupled with an ESI-(Qq)-TOF-MS 6520 detector; Agilent Technologies, Santa Clara, CA). Separation was carried out at 25 °C using a Purospher StarRP-18e (5 μm, 150 × 4.6 mm) column from Merck (Darmstadt, Germany). Gradient elution at 1 mL min^{-1} with a methanol/water + 0.1% HCOOH (20–70%) mobile phase between 0 and 15 min and 90% methanol up to 20 min was performed. The methanol was supplied by Burdick–Jackson (Muskegon, MI), and the HCOOH was obtained from Aldrich (St. Louis, MO). The injection volume was 100 μL.

ESI-TOF-MS was performed in negative ionisation mode (ESI(−)) with nitrogen as the drying gas at 11 L min^{-1} while applying a TOF fragmentor voltage of 175 V, a capillary voltage of 3500 V over an m/z range of 50–500, a gas temperature of 350 °C, and a nebuliser pressure of 60 psi. The concentration decay of CA was obtained from a calibration curve with $r^2 = 0.9957$ and a limit of confidence of 95%. The calibration curve was determined over a linear concentration range from 1 to 100 mg L^{-1} of CA. Solutions above the concentration of the calibration range were diluted.

3. Results and discussion

3.1. Description of the TiO_2/C800 composite

The TiO_2/C800 composite was a black powder. Its density was higher than the densities of the corresponding precursors, i.e., the raw residue and TiO_2. The composite's surface ($pH_{pzc} = 3.5$) was remarkably acidic compared with that of the carbonaceous support ($pH_{pzc} = 11.4$).

The immobilisation of the TiO_2 on carbon affected the textural characteristics of the support prepared using *manihot* residues, as demonstrated by measuring the N_2 adsorption–desorption isotherms. According to the IUPAC classification system, the carbon sample C800 displayed a hybrid isotherm (figure not shown here) of type I–II, which is typical for materials with a considerable degree of microporosity. This nitrogen adsorption isotherm contrasted significantly with the isotherm exhibited by the bare TiO_2 before immobilisation, whereas the isotherm of the composite occupied an intermediate position. As expected, the presence of crystalline TiO_2 and its agglomerates drastically reduced the specific surface area of the composite (200 m^2 g^{-1}) relative to that of the carbonaceous support (434 m^2 g^{-1}), mainly due to the obstruction of the carbon micropores. This reduction was confirmed by a decrease in the micropore volume from 61% to 28%.

The surface composition obtained from the EDS spectrum of the composite indicated the presence of titanium, carbon and the intrinsic elements of the plant *manihot*. An SEM micrograph of the composite demonstrated that isolated TiO_2 nano-agglomerates were attached to the surface of the carbon. This finding suggests that adsorption and photocatalysis phenomena may occur simultaneously due to the low loading of TiO_2 onto the carbon. In contrast, in the studies of Mahmoodi et al. (2011), it was observed that TiO_2 particles entirely covered the surface of sodium alginate, and that composite was used in the investigation of the adsorption and degradation of the anthraquinonic dye acid green 25. By using glycerol, Sreethawong, Ngamsinlapasathian, and Yoshikawa (2012) observed the formation of uniform TiO_2 nanoparticles in the form of clusters.

3.2. Adsorption of carminic acid

Fig. 1 illustrates the isotherms describing the adsorption of CA onto TiO_2, the raw *manihot* residues and the carbon sample C800 after 24 h of contact. The values of the Freundlich constant (k_F) were 19.7 and 4.0 mg g^{-1}/(mg L^{-1})$^{1/n}$ for TiO_2 and carbon C800, respectively. According to the Freundlich equation, the energy of adsorption decreases with the occupation of active sites. Values of $1/n$ less than one indicate an adsorbent with high energetic heterogeneity. Both the semiconductor TiO_2 and carbon C800 exhibited similar heterogeneity factors of 0.23 and 0.26, respectively. The corresponding saturation capacity was calculated by the non-linear form of the Langmuir equation, and the respective results were 70 mg g^{-1} for TiO_2 and 40 mg g^{-1} for carbon C800. Our materials were saturated with lower amounts of CA than those required to saturate a weak anion exchange resin (Cabrera & Fernandez-Lahore, 2007) and polymeric particles (Bibi et al., 2012). In contrast, the extent of CA adsorbed by the TiO_2 and carbon was higher than that adsorbed by glass powder (Atun & Hisali, 2003). The adsorption isotherms in Fig. 1 demonstrate that both the semiconductor TiO_2 and the carbon separately retained the dye. Moreover, the desorption of 4% (0.3 μmol m^{-2}) CA from carbon is feasible with water (see inset in Fig. 1). This property allows CA to concentrate on the surface of the composite by adsorption and allows for the further decomposition of desorbed CA by TiO_2 under irradiation.

The strong adsorption of CA onto TiO_2 can be explained by the same mechanism as that exhibited by anionic azo dyes, and depending on the position and number of ionised hydroxyl groups, mono- and bidentate adsorption complexes can be formed (Bao et al., 2013). Adsorption occurs as a result of interactions between the negatively charged CA ($pK_{a,1} = 1.6 \pm 0.2$) and the $TiOH_2^+$ semiconductor sites at a pH of 5.7, which is slightly lower than the pH_{pzc} of 6.25 of titanium dioxide (Behnajady, Yavari, & Modirshahla, 2014). Although other reported values for the $pK_{a,1}$ of CA exist, 2.81 (Jørgensen & Skibsted, 1991; Rasimas, Berglund, & Blanchard, 1996) and 3.13 (Reyes-Salas et al., 2011), all of the corresponding studies support the fact that CA exists in an anionic form in a solution of deionised water without pH adjustment. The same explanation applied to the adsorption of CA on C800, in which $pH < pH_{pzc}$ once again because the carbon exhibits basic type H (Valix, Cheung, & McKay, 2004) character with a pH_{pzc} of 11.4. However, the adsorption isotherms in Fig. 1 show that the

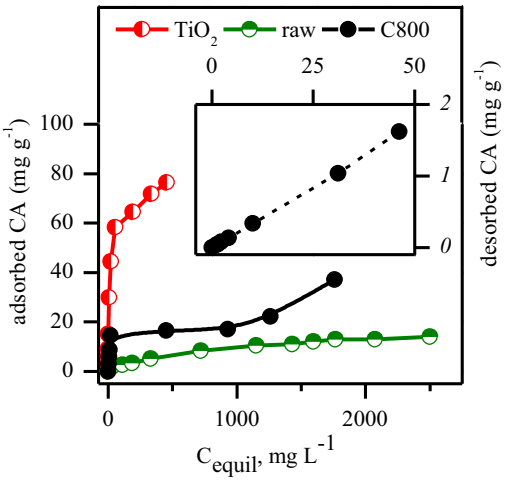

Fig. 1. Adsorption and desorption (inset) isotherms of CA from an aqueous solution on TiO_2, raw *manihot* residues, and the carbonaceous support C800 of the composite.

carbon C800 adsorbs less CA than does TiO_2, although its specific surface area is nearly eight times larger than that of TiO_2. A possible explanation is the degree of microporosity of the carbon. The molecular size of CA (ω = 4.57 nm^2, Antonio-Cisneros, 2010) makes it difficult for it to penetrate the micropores, which contributes to 61% of the specific surface area of C800.

Finally, we aimed to demonstrate the relative adsorption affinities of the semiconductor TiO_2, carbon, and the composite upon the adsorption of CA at moderate concentrations (300 mg L^{-1}) in the short period planned for the photolysis and photocatalytic experiments. When a CA solution was measured photometrically after 90 min of contact with the three different materials, the band at 450–550 nm in Fig. 2A indicates that adsorption occurred on the Degussa TiO_2 to a greater extent than on the carbon sample C800 (Fig. 2B) and the composite (Fig. 2C) under the same conditions. This finding corroborates the results presented in Fig. 1. Due to the basicity (pH_{pzc} = 11.4) of the carbon, a bathochromic effect on the Vis-band of the CA solutions was observed (Fig. 2B).

3.3. Photodegradation of CA under UV-lamp irradiation in the presence of a TiO_2/C800 composite

Fig. 2D–F depicts the UV–Vis spectra of the irradiated CA solutions at 254 nm after 90 min of contact with the composite under different temperature and environmental conditions. As shown, the prepared TiO_2/C800 composite exhibited a low decomposition rate toward the dye in air at 15 °C (Fig. 2D). At 50 °C, CA decomposed readily and to an even greater extent in air (Fig. 2E) than in nitrogen (Fig. 2F), due to the presence of oxygen. These spectra allow for the monitoring of the photolytic and photocatalytic decomposition rate of CA under the conditions studied, as shown in Fig. 3A. The photolysis and photocatalysis kinetic curves exhibited *pseudo*-first order behaviour, and the parameters were calculated by non-linear regression. Table 1 shows the values of the rate constants, which indicate that the photocatalysis of the CA was favoured at the applied temperature, as expected. For comparison, a photocatalytic experiment using the bare semiconductor TiO_2 is also presented. The degradation rate exhibited by the composite in air was higher than that in the presence of N_2, and the highest rate constant was obtained in the experiment with TiO_2, which was not surprising. However, the advantage of using the

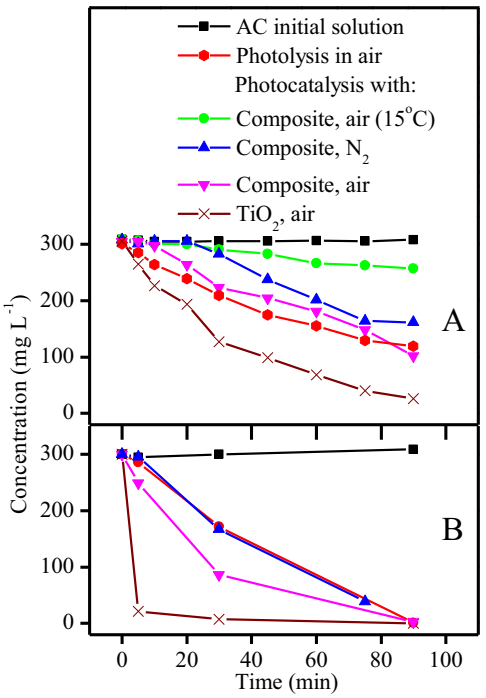

Fig. 3. Concentration decay of CA subjected to photolysis and photocatalysis at 50 °C under different atmospheres in the presence of the composite and TiO_2. The kinetic curves were measured by UV–Vis at 432 nm (A) and by LC/QTOF-MS (B).

Table 1
Kinetic rate constants of the *pseudo*-first order photodegradation of CA measured by UV–Vis and LC-ESI/QTOF-MS.

Process	System conditions	$k_1 \times 10^{-2}$ (min^{-1}) measured by	
		UV–Vis	LC–MS
Photolysis	In air at 50 °C	1.1	2.4
Photocatalysis	With composite in air at 15 °C	0.2	–
	With composite in N_2 at 50 °C	0.7	2.4
	With composite in air at 50 °C	1.0	4.2
	With TiO_2 in air at 50 °C	2.6	52.7

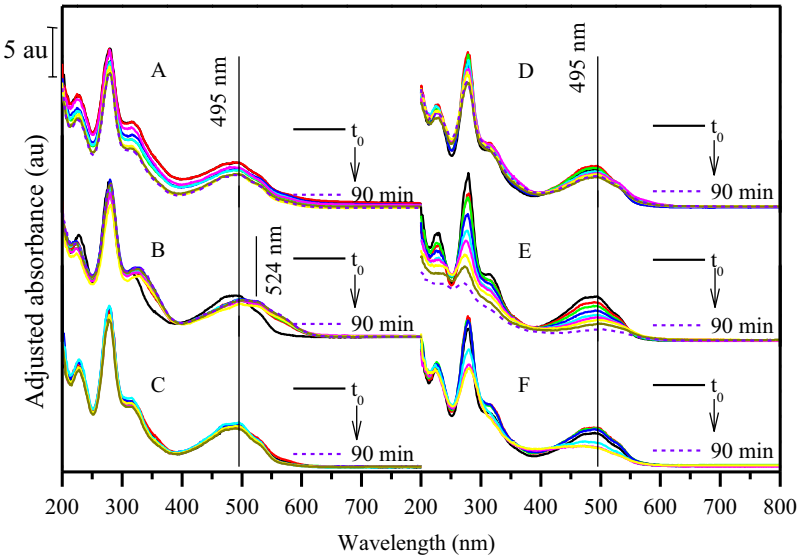

Fig. 2. UV–Vis spectroscopic monitoring of a solution of CA (300 mg L^{-1}) during adsorption (A–C) on TiO_2 (A), carbon C800 (B) and the composite (C) and subjected to photocatalysis (D–F) for 90 min in the presence of the composite at 15 °C in air (D), at 50 °C in air (E) and at 50 °C in N_2 (F).

composite over titanium dioxide nanoparticles is the ability to recover the solid material, in which case, the solution to be analysed is free of suspended matter. The TiO_2 nanoparticles formed aggregates on the carbon surface, and the content of the photocatalytic material in the composite (2 mg of pure TiO_2 in 10 mg of composite) was much lower than in the experiment with titanium dioxide (10 mg of pure TiO_2). Nevertheless, the composite was capable of decomposing approximately 50% of the CA in 90 min under different conditions.

The progress of the photocatalytic reaction under different conditions was also monitored by HPLC, as shown in Fig. 3B. The first-order rate constants calculated from the HPLC concentration data are significantly different from the values of k_1 obtained by UV–Vis spectroscopy (see Table 1). Although UV–Vis spectroscopy measured the signal of the compounds in the bulk, HPLC separated the coloured decomposition products of CA from the dye peak and allowed for the quantification of the individual compounds of interest using a calibration curve. Although no correlation between the adsorption of anthraquinonic dyes and their photodegradation rate was found in the work of Baran et al. (2008), our experiments demonstrated that the photodegradation rate constant of CA was much higher with TiO_2 (see the last column in Table 1), which adsorbed CA to a greater extent than the composite did (compare Fig. 2A and C). Another unforeseen result was the fact that after 90 min of treatment, the CA itself decomposed almost completely in the presence of both TiO_2 and the composite in air and in nitrogen (compare Fig. 3B with A). This finding could only be made with the help of chromatography and will be discussed in the next section.

3.4. Photodegradation intermediates of CA detected under UV irradiation by LC/QTOF-MS

For the identification of uncoloured and coloured intermediates, we analysed aliquots by LC-ESI/QTOF-MS during the photocatalytic experiments with the composite. Fig. 4 shows three selected chromatograms. The structures of the photodegradation products of CA are presented in Table 2. The intermediates mainly conserved the anthraquinone moiety (with $\lambda_{max,1}$ = 250 nm and $\lambda_{max,2}$ = 325 nm), with the hydroxyl groups acting as auxochromes, which in conjugation with the π electrons of the anthraquinone core might increase λ_{max} to a wavelength similar to that of CA. During photocatalysis, this phenomenon produces a decrease in the band at 495 nm measured by UV–Vis spectroscopy, which does not correspond to CA itself but to a mixture of degradation products. Instead, the concentration fate of CA observed by HPLC by means of a single peak at a defined retention time is unaffected by the contribution of the products. As indicated by the comparison of Fig. 3A and B, in analysing the treated solution, the decrease in the concentration of CA is actually faster when using HPLC than UV–Vis analysis. This discrepancy explains why the rate constants for the kinetics of the decomposition of the dye itself assessed by HPLC are higher than those determined by UV–Vis spectroscopy.

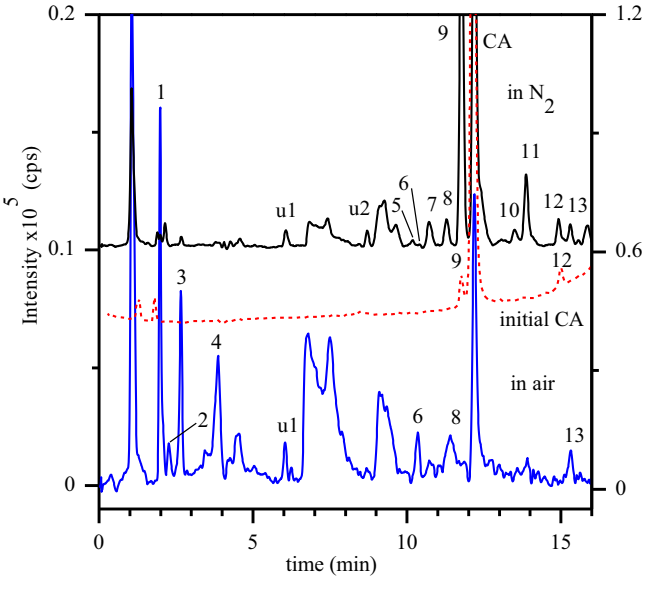

Fig. 4. TIC obtained from LC–MS analysis of the stock solution (dotted line, right axis) of CA (300 mg L^{-1}) after 90 min of photocatalytic treatment with the composite under nitrogen (right axis) and air (left axis) at 50 °C. The chromatographic conditions are described in the experimental section. Peaks correspond to the identified products P1–P13 gathered in Table 2. Chromatograms were shifted upwards from their baselines for better viewing.

At least nine new peaks of considerable intensity eluted prior to the appearance of the dye peak in the chromatogram (Fig. 4) of the aliquot analysed during the photocatalytic experiment. The peaks that are numbered in the figure correspond to the intermediate products obtained using the composite, and they exhibit a defined isotopic pattern. Table 2 presents the retention times, exact masses of the molecular ions (m/z), error values (Δm), and proposed structures for 13 of the products detected in Fig. 4. The chromatogram labelled "initial CA" in Fig. 4 shows that peaks 9 and 12 existed in low amounts in the starting CA reagent.

The accurate identification of the aforementioned structures indicates that under the applied photocatalytic conditions (90 min of irradiation at 254 nm, under air at 50 °C), the TiO_2/C800 composite tended to not completely decompose the dye molecule. The products listed in Table 2 indicate that the breakage of the CA molecule yields mainly the glucopyranosyl-dioxoanthracene moiety with different degrees of hydroxylation, with and without the original carboxylic group. Only four compounds (peaks 1–4) corresponded to the aglycone moiety of the CA structure. The peaks marked u1 and u2 in Fig. 4 correspond to unknown products whose structures could not be assigned, although well-defined mass spectra were obtained, and these peaks corresponded to masses of 255.2349 and 463.0906, respectively. The binuclear compound (peak 4) eluting at 3.86 min was only detected in the aliquot collected in an oxygen-rich atmosphere. The faster decomposition of CA in the presence of air compared to that in nitrogen (see Fig. 3B) could be responsible for this result. Correspondingly, intermediates 10–12 are absent in the chromatogram of the 90-min aliquot shown in Fig. 4 because they transformed faster in air into compounds free of the sugar moiety, such as those represented by peaks 1–4. Thus, the intensities of peaks 1–3 are higher in the chromatogram of the sample collected from the experiment performed in air.

The masses corresponding to peaks 2, 3 and 5 were also detected in beverages during the photodegradation process (Gosetti et al., 2015). The structures proposed by the authors for those masses might derive from the interactions between CA and the emulsifiers contained in the beverages. This can explain the different structure proposed by us and in the work of Gosetti et al. (2015) for the nominal masses 207 (peak 3) and 237 (peak 2). Since we performed photocatalytic experiments of CA, we propose oxidation of one hydroxyl group in the glycopyranoside substituent to yield the nominal mass of 489 (peak 5), however the exact position (C2, C3 or C4) of the keto group cannot be determined by LC–MS.

Interestingly, four peaks exhibiting a nominal mass m/z_{exper} of 475 were detected. In this case, the structures of the pairs 7 & 8 and 9 & 11 were assigned by considering the log P values presented in the last cells of Table 2. The pair 7 & 8 corresponds to a molecule in which the glucosyl substituent carries three hydroxyl groups instead of four as in CA, i.e., the substituent corresponds to a

Table 2
Retention time, molecular mass and possible structures identified by LC-ESI-Qq-TOF-MS of metabolites of CA produced after 90 min of irradiation (254 nm) at 50 °C on a TiO_2/C800 composite. The peak numbering is as in the chromatograms of Fig. 4.

Proposed structure	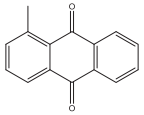	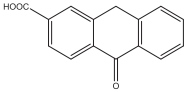	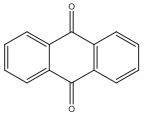	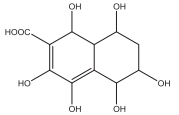		
Peak no.	1	2	3	4		
t_R (min)	1.97	2.25	2.64	3.86		
Formula	$C_{15}H_{10}O_2$	$C_{15}H_{10}O_3$	$C_{14}H_8O_2$	$C_{11}H_{14}O_8$		
m/z_{exper}	221.0623	237.0576	207.0461	273.0635		
m/z_{calc}	221.0608	237.0557	207.0451	273.0616		
Δm	6.79	8.01	4.83	6.96		
Detected in	N_2, air	N_2, air	N_2, air	Air		
Proposed structure	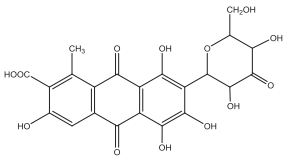	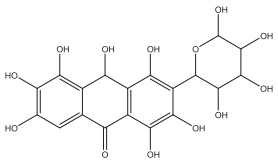	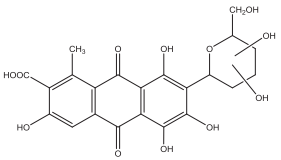	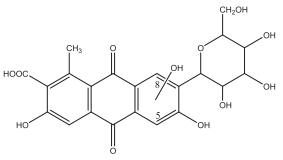		
Peak no.	5	6	7	8	9 = dcII	11
t_R (min)	10.172	10.35	10.71	11.29	11.73	13.86
Formula	$C_{22}H_{18}O_{13}$	$C_{19}H_{18}O_{13}$	$C_{22}H_{20}O_{12}$		$C_{22}H_{20}O_{12}$	
m/z_{exper}	489.0686	453.0683	475.0896		475.0900	
m/z_{calc}	489.0674	453.0674	475.0882		475.0882	
Δm	2.45	1.99	2.95		3.79	
Detected in	N_2	N_2, air	N_2	N_2, air	N_2	N_2
Proposed structure	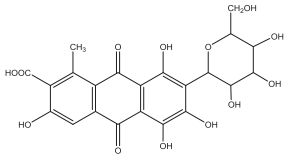	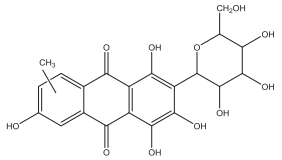	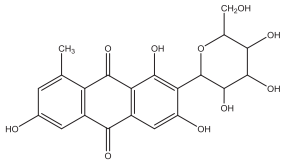			
Peak no.	CA	10 and 13		12	log *P* 7 and 8	9 and 11
t_R (min)	12.20	13.52	15.29	14.91	−1.38	0.93
Formula	$C_{22}H_{20}O_{13}$	$C_{21}H_{20}O_{11}$	$C_{21}H_{20}O_{11}$	$C_{21}H_{20}O_{10}$		
m/z_{exper}	491.0852	447.0937	447.095	431.1		
m/z_{calc}	491.0831	447.0933	447.0933	431.0983		
Δm	4.28	0.89	3.80	3.94		
Detected in	–	N_2	N_2, air	N_2		

deoxyglucose moiety. This finding indicates that under the applied conditions, the photocatalytic process removes one hydroxyl group at this site from the CA molecule, but such removal can occur at any position of the glucosyl substituent. Indeed, this removal is probably the reason why two peaks, 7 and 8, exhibited the same $\Delta m/z$ of 475. The different position of the hydroxyl substituent in the deoxyglucosyl moiety could shift the retention times of the two isomers due to intramolecular bonding. Furthermore, the hydrophilicity of the aglycone/glycone moieties of biologically active compounds determines the extent of chromatographic retention (Davydov, Elizalde Gonzalez, & Kiselev, 1982) and explains why, in this case, the pair 7 & 8 elutes before the pair 9 & 11.

The first possible identity of the structure of the compounds eluting as peaks 9 & 11 is 7-*C*-glucopyranosyl flavokermesic acid, with the hydroxyl group in position 8 (C-8-OH) of the anthraquinone ring. This derivative of CA has been labelled dcII (from the insect *Dactylopius coccus*) and has been detected in historical objects (Stathopoulou, Valianou, Skaltsounis, Karapanagiotis, & Magiatis, 2013). Although Peggie, Hulme, McNab, and Quye (2008) did not define the stereochemistry of the glycosidic linkage, Lech and Jarosz (2011) proposed an α–D-glucopyranosyl derivative of flavokermesic acid for dcII. The second possibility for the identity of dcII is the molecule 7-*C*-glucopyranosyl flavokermesic acid with the hydroxyl group in position 5 (C-5-OH) of the anthraquinone moiety. According to Peggie et al. (2008), this alternative is unlikely in cochineal insects, but it cannot be neglected as a photoproduct. Finally, C-8-OH eluted very close to but before the CA peak in Stathopoulou's work (2013), and we can assume that, in our case, it appeared as peak 9 and not as peak 11 in Fig. 4. However, any assignment of the isomers C-8-OH and C-5-OH would be speculation. Compound 12, with $m/z = 475 - 44\ (CO_2) = 431$, is the only case of decarboxylation of the anthraquinone core of dcII.

As described in the work of Brack et al. (2003), anthracene modified its structure under sunlight, yielding polyaromatic quinones and hydroxyquinones, similar to those reported here for the photodegradation of CA. Brack et al. reported organism-dependent toxicity and genotoxicity. In particular, anthracene-9,10-dione (peak 3 in Fig. 4 and Table 2) was reported to have caused 57% inhibition of the algal reproduction of the unicellular green alga *Scenedesmus vacuolatus* (Brack et al., 2003). This result may be important with respect to the photolysis of CA in wastewater from the food industry. Furthermore, to visualise the effect of incomplete mineralisation, we followed the formation of intermediates by LC–MS and detected this deleterious photodegradation compound.

4. Conclusions

A composite material with photocatalytic activity was obtained from the plant stems of *M. dulcis*, a major agricultural residue. Aggregates of TiO_2 nanoparticles on carbon combine the adsorption capability and catalytic activity of both materials, respectively. The composite particle size allows for better handling in photocatalytic systems than that possible using TiO_2 alone. On the other hand, *manihot* carbon has a basic pH_{pzc} and a large surface area, which allows for the adsorption of significant amounts of anionic compounds such as carminic acid. Moreover, the adsorption is reversible, and the dye can be partially recovered by desorption, which can be advantageous in the case of artisanal carpeting effluents. Desorption is also a step that can play an important role in the action of the photocatalyst. Intermediate products detected during photodegradation indicate that the dye can generate toxic by-products, in contrast to the nature of the dye, which is considered safe. Using LC/QTOF-MS, 13 photodegradation products were identified, most of which contained the group glucopyranosyl-dioxoanthracene with different degrees of hydroxylation. The degradation products generated during photocatalysis depend on the atmosphere in which the process is carried out. In the presence of air, we observed fewer products than in a N_2 atmosphere due to the faster decomposition of CA favoured by an oxygen-rich atmosphere. The deleterious compound anthracene-9,10-dione was detected both in N_2 and in air.

Acknowledgements

This work was supported by the following research projects: CONACYT CB-2008-01-100439, and INFR-123779-2009. We thank the financial funding of the university (UAP) for the last project. CMAC is grateful for the grant (227566) received from CONACYT – Mexico.

References

Ahmed, S., Rasul, M. G., Martens, W. N., Brown, R., & Hashib, M. A. (2011). Advances in heterogeneous photocatalytic degradation of phenols and dyes in wastewater: A review. *Water Air and Soil Pollution, 215*, 3–29.

Akpan, U. G., & Hameed, B. H. (2009). Parameters affecting the photocatalytic degradation of dyes using TiO_2-based photocatalysts: A review. *Journal of Hazardous Materials, 170*, 520–529.

Antonio-Cisneros, C. M. (2010). *DSc. Thesis*. México: Universidad Autónoma de Puebla.

Antonio-Cisneros, C. M., & Elizalde-González, M. P. (2010). Characterization of *Manihot* residues and preparation of activated carbon. *Biomass and Bioenergy, 34*, 389–395.

Arroyo-Figueroa, G., Ruiz-Aguilar, G. M. L., López-Martínez, L., González-Sánchez, G., Cuevas-Rodríguez, G., & Rodríguez-Vázquez, R. (2011). Treatment of a textile effluent from dyeing with cochineal extracts using Trametes versicolor fungus. *The Scientific World Journal, 11*, 1005–1016.

Asiltürk, M., & Şener, S. (2012). TiO_2 – activated carbon photocatalysts: Preparation, characterization and photocatalytic activities. *Chemical Engineering Journal, 180*, 354–363.

Atun, G., & Hisarli, G. (2003). Adsorption of carminic acid, a dye onto glass powder. *Chemical Engineering Journal, 95*, 241–249.

Baran, W., Makowski, A., & Wardas, W. (2008). The effect of UV radiation absorption of cationic and anionic dye solutions on their photocatalytic degradation in the presence TiO_2. *Dyes and Pigments, 76*, 226–230.

Bao, N., Li, Y., Yu, X. H., Niu, J. J., Wu, G. L., & Xu, X. H. (2013). Removal of anionic azo dye from aqueous solution via an adsorption-photosensitized regeneration process on a TiO_2 surface. *Environmental Science and Pollution Research, 20*, 897–906.

Behnajady, M. A., Yavari, S., & Modirshahla, N. (2014). Investigation on adsorption capacity of TiO_2-P25 nanoparticles in the removal of a mono-azo dye from aqueous solution: A comprehensive isotherm analysis. *Chemical Industry & Chemical Engineering Quaterly, 20*, 97–107.

Bibi, N. S., Galvis, L., Grasselli, M., & Fernández-Lahore, M. (2012). Synthesis and sorption performance of highly specific imprinted particles for the direct recovery of carminic acid. *Process Biochemistry, 47*, 1327–1334.

Bourikas, K., Vakros, J., Kordulis, C., & Lycourghiotis, A. (2003). Potentiometric mass titrations: Experimental and theoretical establishment of a new technique for determining the point of zero charge (PZC) of metal (Hydr)oxides. *Journal of Physical Chemistry B, 107*, 9441–9451.

Brack, W., Altenburger, R., Küster, E., Meissner, B., Wenzel, K. D., & Schüürmann, G. (2003). Identification of toxic products of anthracene photomodification in simulated sunlight. *Environmental Toxicology and Chemistry, 22*, 2228–2237.

Cabrera, R. B., & Fernandez-Lahore, H. M. (2007). Primary recovery of acid food colorant. *International Journal of Food Science and Technology, 42*, 1315–1326.

Chen, Y. X., Luo, B. H., Zhao, B. Y., Lai, Y. J., Wang, H. Z., Gao, M. Y., Zhang, W. X., & Chen, K. B. (2012). Method to control the phase of TiO_2 in porous carbon–TiO_2 composite. *Journal of Inorganic and Organometallic Polymer Materials, 22*, 90–96.

Davydov, V. Ya., Elizalde Gonzalez, M. P., & Kiselev, A. V. (1982). Correlation between the retention of cardiac glycosides in reversed-phase high-performance liquid chromatography a diphenylsilyl stationary phase, the structure of their molecules and their biological activity. *Journal of Chromatography A, 248*, 49–62.

Foo, K. Y., & Hameed, B. H. (2010). Decontamination of textile wastewater via TiO_2/activated carbon composite materials. *Advances in Colloid and Interface Science, 159*, 130–143.

Gosetti, F., Chiuminatto, U., Mazzucco, E., Mastroianni, R., & Marego, E. (2015). Ultra-high-performance liquid chromatography/tandem high resolution mass spectrometry analysis of sixteen red beverages containing carminic acid: Identification of degradation products by using principal component analysis/discriminant analysis. *Food Chemistry, 167*, 454–462.

Huang, D., Miyamoto, Y., Matsumoto, T., Tojo, T., Fan, T., Ding, J., Guo, Q., & Zhang, D. (2011). Preparation and characterization of high-surface-area TiO_2/activated carbon by low-temperature impregnation. *Separation and Purification Technology, 78*, 9–15.

Jørgensen, K., & Skibsted, L. H. (1991). Light sensitivity of cochineal. Quantum yields for photodegradation of carmine acid and conjugate bases in aqueous solution. *Food Chemistry, 40*, 25–34.

Koperska, M., Łojewski, T., & Łojewska, J. (2011). Vibrational spectroscopy to study degradation of natural dyes. Assessment of oxygen-free cassette for safe exposition of artefacts. *Analytical and Bioanalytical Chemistry, 399*, 3271–3283.

Körbahti, B. K., & Rauf, M. A. (2009). Determination of optimum operating conditions of carmine decoloration by UV/H2O2 using response surface methodology. *Journal of Hazardous Materials, 161*, 281–286.

Leary, R., & Westwood, A. (2011). Carbonaceous nanomaterials for the enhancement of TiO_2 photocatalysis. *Carbon, 49*, 741–772.

Lech, K., & Jarosz, M. (2011). Novel methodology for the extraction and identification of natural dyestuffs in historical textiles by HPLC-UV-Vis-ESIMS. Case study: chasubles from the Wawel Cathedral collection. *Analytical and Bioanalytical Chemistry, 399*, 3241–3251.

Mahmoodi, N. M., Arami, M., & Zhang, J. (2011). Preparation and photocatalytic activity of immobilized composite photocatalyst (titania nanoparticle/activated carbon). *Journal of Alloys and Compounds, 509*, 4754–4764.

Matos, J., Chovelon, J. M., Cordero, T., & Ferronato, C. (2009). Influence of surface properties of activated carbon on photocatalytic activity of TiO_2 in 4-chlorophenol degradation. *Open Environmental Engineering Journal, 2*, 21–29.

Peggie, D. A., Hulme, A. N., McNab, H., & Quye, A. (2008). Towards the identification of characteristic minor components from textiles dyed with weld (*Reseda luteola* L.) and those dyed with Mexican cochineal (*Dactylopius coccus* Costa). *Microchimica Acta, 162*, 371–380.

Rangabhashiyam, S., Anu, N., & Selvaraju, N. (2013). Sequestration of dye from textile industry wastewater using agricultural waste products as adsorbents. *Journal of Environmental Chemical Engineering, 1*, 629–641.

Rasimas, J. P., Berglund, K. A., & Blanchard, G. J. (1996). A molecular lock-and-key approach to detecting solution phase self-assembly. A fluorescence and absorption study of carminic acid in aqueous glucose solution. *Journal of Physical Chemistry, 100*, 7220–7229.

Reyes-Salas, O., Juárez-Espino, M., Manzanilla-Cano, J., Barceló-Quintal, M., Reyes-Salas, A., & Rendón-Osorio, R. (2011). Titrimetric and polarographic determination of carminic acid and its quantification in Cochineal (*Dactylopius coccus*) extracts. *Journal of the Mexican Chemical Society, 55*, 89–93.

Sarikaya, R., Selvi, M., & Erkoç, F. (2012). Evaluation of potential genotoxicity of five food dyes using the somatic mutation and recombination test. *Chemosphere, 88*, 974–979.

Sabinas-Hernández, S.A. (2011). MSc. Thesis, Universidad Autónoma de Puebla, México.

Sreethawong, T., Ngamsinlapasathian, S., & Yoshikawa, S. (2012). Glycerol as an efficient mesopore-controlling agent for synthesis of mesoporous-assembled TiO_2 nanocrystals and their remarkable photocatalytic H_2 production activity. *Materials Research Bulletin, 47*, 199–205.

Stathopoulou, K., Valianou, L., Skaltsounis, A. L., Karapanagiotis, I., & Magiatis, P. (2013). Structure elucidation and chromatographic identification of anthraquinone components of cochineal (*Dactylopius coccus*) detected in historical objects. *Analytica Chimica Acta, 804*, 264–272.

Valix, M., Cheung, W. H., & McKay, G. (2004). Preparation of activated carbon using low temperature carbonization and physical activation of high ash raw bagasse for acid dye adsorption. *Chemosphere, 56*, 493–501.